Journal of the European Ceramic Society 7 (1991) 369–378

Oxidation of Pressureless Sintered Si_2N_2O Materials

C. O'Meara,[a] J. Sjöberg,[b] G. Dunlop[a]*

[a] Department of Physics, [b] Department of Inorganic Chemistry, Chalmers University of Technology, S-412 96 Göteborg, Sweden

&

R. Pompe

Swedish Institute for Silicate Research, S-402 29 Göteborg, Sweden

(Received 19 October 1990; revised version received 4 December 1990; accepted 21 December 1990)

Abstract

The oxidation behaviour of pressureless sintered Si_2N_2O materials prepared from both amorphous and crystalline starting powders has been examined. The materials exhibited excellent oxidation resistance at temperatures of up to 1350°C. Thin protective oxide scales formed which had a duplex morphology after long exposures to air at high temperatures. Substantial crystallisation of the intergranular glass phase with formation of $Y_2Si_2O_7$ occurred during oxidation at 1200°C and 1350°C. Catastrophic oxidation occurred at temperatures $\geq$ 1400°C. This behaviour is enhanced by an oxidation-induced shift in the composition of the material to a liquid-forming region in the Y–Si–Al–O–N system.

Aus amorphen und kristallinen Ausgangspulvern wurden drucklos Si_2N_2O-Werkstoffe gesintert, deren Oxidationsverhalten untersucht wurde. Die Werkstoffe zeigten bis zu 1350°C eine ausgezeichnete Oxidationsbeständigkeit. Bei hohen Temperaturen bildeten sich nach langer Auslagerung an Luft dünne, zweischichtige oxidische Schutzschichten. Während der Oxidation bei 1200°C und bei 1350°C kristallisierte die intergranulare Glasphase unter Bildung von $Y_2Si_2O_7$ aus. Über 1400°C verläuft die Oxidation katastrophal. Dieses Verhalten wird durch eine durch die Oxidation bedingte Verschiebung der Zusammensetzung im Y–Si–Al–O–N System verstärkt.

On a étudié l'oxydation de matériaux Si_2N_2O consolidés par frittage naturel, la poudre de départ étant sous forme amorphe ou cristalline. Les matériaux présentent une très bonne résistance à l'oxydation pour des températures allant jusqu'à 1350°C. Des couches protectrices minces d'oxyde sont formées, possèdant une morphologie duplex après une longue exposition à l'air à haute température. Lors de l'oxydation à 1200 et 1350°C, la phase vitreuse intergranulaire cristallise de manière importante, en formant du $Y_2Si_2O_7$. Pour des températures $\geq$ 1400°C on observe une oxydation catastrophique. Ce comportement est accentué par un décalage de composition du matériau, provoqué par l'oxydation, vers un domaine de formation de liquide du système Y–Si–Al–O–N.

1 Introduction

Silicon oxynitride (Si_2N_2O) is a promising candidate high-performance ceramic material which has thermo-mechanical properties similar to those of other nitrogen ceramics.[1–4] The main advantage of Si_2N_2O is claimed to be its improved resistance to oxidation and to molten non-ferrous metals and salts.[5] However, the development of the material as a high-performance ceramic has been slow, due to the lack of commercial sinterable powders and also because of difficulties in obtaining fully dense bodies. The latter problem occurs because Si_2N_2O tends to decompose at the required sintering temperatures (1700–1800°C).[6,7] It has recently been shown, however, that dense Si_2N_2O bodies can be produced by pressureless sintering.[8,9] The use of double oxide sintering additives (most commonly Y_2O_3 and Al_2O_3) lowers the eutectic temperature of the liquid-phase sintering medium and good densi-

* Present address: Department of Mining and Metallurgical Engineering, The University of Queensland, Queensland 4072, Australia.

Journal of the European Ceramic Society 0955-2219/91/$3.50

fication can be achieved in the 1600–1700°C temperature range.[8]

This paper examines the behaviour of pressureless sintered Si_2N_2O materials in oxidising environments at temperatures in the range 1000–1500°C. The pure compound Si_2N_2O has an excellent resistance to oxidation which is due to the formation of a protective surface layer of amorphous SiO_2 during the early stages of oxidation.[10–12] With sintered polyphase Si_2N_2O materials a deterioration in the high-temperature oxidation resistance similar to that observed in sintered β-Si_3N_4 materials can be expected. The existence of residual porosity and secondary phases, both crystalline and amorphous, in these materials gives rise to a more complex oxidation behaviour and a lowered resistance to oxidation than for pure β-Si_3N_4.

The materials which were examined in the present work were pressureless sintered from either amorphous or crystalline Si_2N_2O powders with additions of 10 wt% Y_2O_3 and 6 wt% Al_2O_3 as sintering aids. The development of microstructure during sintering of these materials is described in Ref. 9. The materials can be fabricated to lie within the Si_3N_4–Si_2N_2O (or O'-phase)–$Y_2Si_2O_7$ compatibility triangle of the Y–Si–Al–O–N system. Compositions within the Si_3N_4–Si_2N_2O–$Y_2Si_2O_7$ triangle have the highest oxidation resistance for this system.[13] All of the end members are chemically compatible with SiO_2 and thus no reaction between the phases should occur before a eutectic involving SiO_2 is reached. For the phases $Y_2Si_2O_7$, Si_2N_2O and SiO_2 this eutectic occurs at ~1500°C[13] and the oxidation resistance should be good up to this temperature. However, residual porosity and remnant glassy phases present in the microstructure can be expected to result in lowered oxidation resistance. The aim of this investigation has been twofold: firstly, to examine the oxidation behaviour of the material in the temperature interval 1000–1500°C; and secondly, to examine the extent of crystallisation of the remnant glass phase during isothermal heat-treatments in air.

2 Experimental

2.1 Materials

Pressureless sintered Si_2N_2O materials were fabricated using amorphous (material A) or crystalline (material B) starting powders with 10 wt% Y_2O_3 and 6 wt% Al_2O_3 as sintering additives. The powder preparation, sintering conditions and microstructural details of the two materials are described in Refs 9, 14 and 15.

For the oxidation experiments cylindrical samples, approximately 3 mm diameter by 2 mm thick, were cut from the sintered bodies with an ultrasonic cutter. This particular size and geometry was used to facilitate transmission electron microscopy (TEM). Specimen dimensions were accurately measured in order to determine their surface area and the specimen surfaces were polished with diamond paste.

2.2 Oxidation procedure

The changes in weight of the specimens during oxidation were recorded either by continuous thermogravimetry using a Harrop TG 716 instrument or by weighing the specimen before and after oxidation in a rapid high-temperature furnace. As detailed in Table 1 the specimens were heat-treated in air at temperatures ranging from 1000 to 1500°C and holding times of 1–50 h were used.

2.3 Microstructural characterisation

Following oxidation, characterisation of the surfaces of the specimens was carried out by X-ray diffractometry (Hägg–Guinier and powder method) and scanning electron microscopy (SEM) using both secondary and backscattered modes. Cross-sections of the oxide scales were examined by SEM and elemental analysis was undertaken by electron probe microanalysis (SEM–EPMA).

Microstructural changes which occurred in the core of the material were investigated using analytical transmission electron microscopy in a Jeol 2000 FX TEM/STEM instrument with a Link Systems AN 10000 EDX spectrometer. Procedures for the preparation of thin foil specimens were the same as described previously.[9]

Table 1. Oxidation temperatures, times and recorded weight gains for materials A and B

Temperature (°C)	*Time* (h)	*Weight gain*			
		Per unit surface area (mg cm^{-2})		(%)	
		A	B	A	B
1000	50	0	0	0	0
1100	50	0	0	0	0
1200	10	—	—	—	—
	20	—	—	—	—
	50	0·94	0·61	3·9	3·2
1350	10	0·9	0·8	4·6	4·3
	20	1·0	1·2	5·1	4·7
	50	1·57	1·38	5·3	4·8
1400	10	1·8	1·3	5·6	6·5
	20	3·8	3·09	23	14·5
1500	10	Melts	0·078	—	37
	30	—	0·078	—	37
	50	Melts	Melts	Melts	Melts

Table 2. Microstructural characteristics of materials A and B

Material	*Starting powder*	*Sintered density (%)*	*Pore size (μm)*	*Grain size distribution (μm)*
A	Amorphous	91	0·5–2·0	0·02–1·0
B	Crystalline	94		0·2–10

3 Results

3.1 Starting microstructure

The general microstructure features of the two materials are summarised in Table 2. The sintered materials consisted of a major crystalline Si_2N_2O phase and a minor glass phase that was a remnant from the liquid-phase sintering medium (see Fig. 1). Neither of the materials were fully dense and material A, which had been fabricated from amorphous starting powder, contained micro-sized internal pores which may be related to its lowered sintered density compared with the crystalline-based material B. The grain size and morphology of the Si_2N_2O grains differed between the two materials. Material A had the most uniform microstructure with sub-micron grains which were randomly oriented (Table 2). Material B had a much coarser crystalline microstructure with predominantly micron-sized grains. The intergranular glassy phase in the microstructures of both materials was observed to be phase separated and consisted of Si-rich and Y-rich regions.

3.2 Oxidation kinetics

The weight change data are detailed in Table 1 in the form of both weight gain per unit surface area and as percentage weight change. The presence of porosity in the specimens, however, does not permit estimation of a rate law for oxidation, since no estimation was made of the surface area associated with the pores. Therefore, further analysis of the observed weight changes and possible kinetic regimes is reserved until Section 4, where these changes are examined with reference to the development of the oxide scales and the internal microstructural changes that occurred at given temperatures. It can be noted, however, from Table 1 that the percentage weight increases were significant, indicating the occurrence of internal oxidation. At temperatures $\geq$ 1400°C large weight gains were recorded. For the samples treated at $\leq$1100°C for 50 h no weight gain was observed and consequently no further analysis of these samples was carried out.

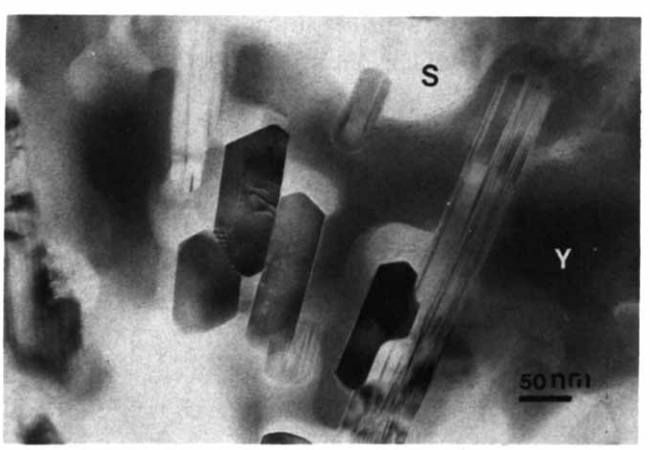

Fig. 1. TEM micrograph of the general microstructure of the as-sintered material A. Sub-micron Si_2N_2O grains are surrounded by a glassy phase that is residual from the sintering process. This amorphous material is phase separated into Y-rich (Y) and Si-rich (S) glasses.

3.3 Characterisation of oxide scales

The identification of oxidation products formed at various temperatures was established from Hägg–Guinier X-ray diffraction patterns of scrapings from the specimen surfaces by X-ray diffraction (powder method) of the oxidised surfaces of bulk specimens. The phases that were identified are detailed in Table 3.

Table 3. Phase content of the oxide scales of materials A and B as identified by X-ray diffractometry

Temperature (°C)	*Phase content*
1 200–1 350	$Y_2Si_2O_7$, amorphous
1 400–1 500	α- and β-SiO_2, amorphous, traces of $Y_2Si_2O_7$

Using SEM the development of oxide scales was found to be very similar for the heat-treatments at temperatures of 1200°C and 1350°C while at temperatures > 1400°C a different oxidation response was observed to occur. The development of oxide scales in these two temperature groupings will be treated separately.

3.3.1 1200°C and 1350°C

In general no difference in the appearance of the oxide scale or its phase content (Table 3) could be observed between materials A and B. The surfaces of specimens that had been oxidised for 10, 20 and 50 h at 1350°C are shown in the series of scanning electron micrographs in Fig. 2. The scales of both materials developed as follows:

10 h: After 10 h at the oxidising temperature the scales had an uneven topography

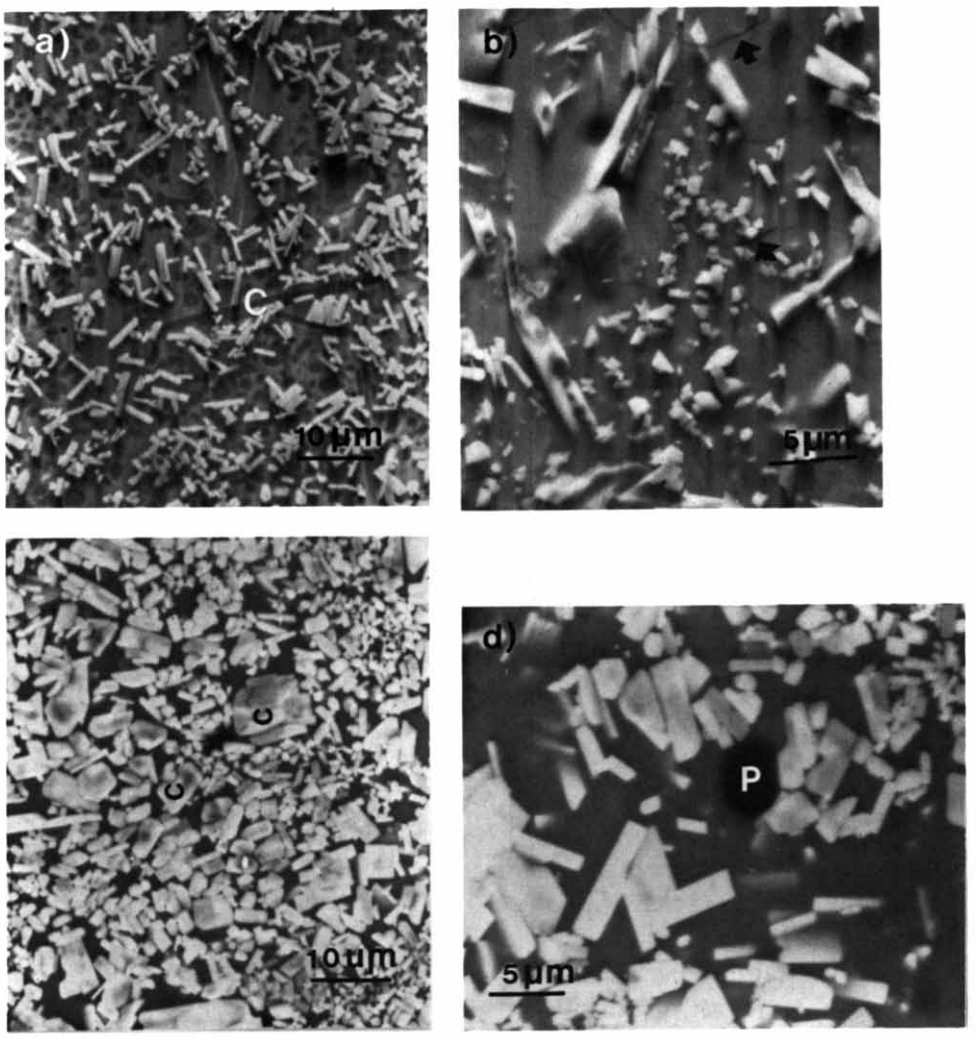

Fig. 2. SEM backscattered images of the oxide surfaces of materials oxidised at 1350°C for 10 h ((a) and (b)) and 50 h ((c) and (d)). (a) Crystalline $Y_2Si_2O_7$ in a mixed silicate amorphous phase. The dark contrasting structures (C) are probably cristabolite (SiO_2). (b) Needle and irregularly shaped $Y_2Si_2O_7$ crystals embedded in the oxide scale. Note the surface cracks (arrows). (c) A high density of $Y_2Si_2O_7$ crystals (C) in the oxide scale after long oxidation exposures. The amorphous phase surrounding the crystals is rich in Si. (d) Gas pores (P) in the scale surfaces indicating that the scale had a high viscosity.

and small cracks were frequently seen on the surfaces (Fig. 2(a) and (b)). The scales consisted of crystalline $Y_2Si_2O_7$ in a mixed silicate amorphous phase. Needle and irregularly shaped crystals often emerged from the surface giving it an uneven topography. Small amounts of a dark contrasting structure, crystalline in form, were also present within the scales. These were possibly crystalline SiO_2 (cristabolite). The most probable reason for cracking in the oxide scale is the difference in thermal expansion coefficients of the various components of the scale. In cross-section the oxide scales were seen to have grown to up to $\sim 10\,\mu m$ in thickness after 1 h and the $Y_2Si_2O_7$ crystals were dispersed through its depth (Fig. 3(a)). The mixed silicate amorphous phase contained mainly Si, Y and Al together with traces of Fe, K and Na impurity element. Gas bubbles, most probably from evolution of nitrogen gas, could be seen both at the matrix–oxide interface and in the surface oxide (Fig. 3(b)). This indicates that the amorphous material in the scale had a high viscosity.

20–50 h: The scales appeared to be continuous and formed a smooth surface in which no cracking was observed (Fig. 2(c) and (d)). The number density of the $Y_2Si_2O_7$ crystals increased with time resulting in well-formed plate-like grains, which indicates that both the nucleation and growth of this phase occurred at the

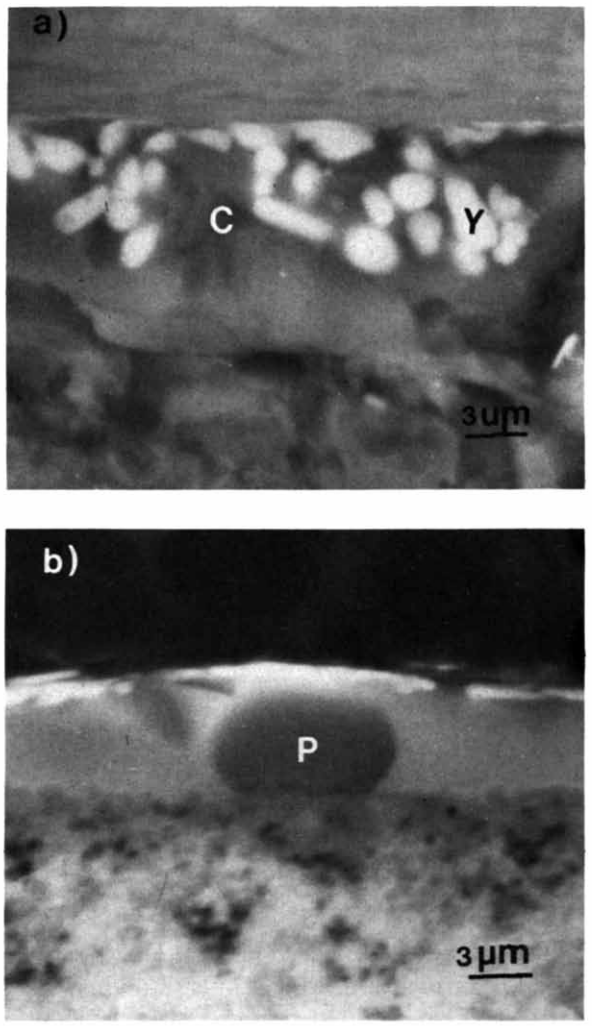

Fig. 3. SEM backscattered images of transverse sections of scales formed after 10 h at (a) 1200°C and (b) 1350°C showing (a) $Y_2Si_2O_7$ crystals (Y) and possibly SiO_2 crystals (C) dispersed in a mixed silicate amorphous phase; (b) nitrogen gas pores (P) in the scale.

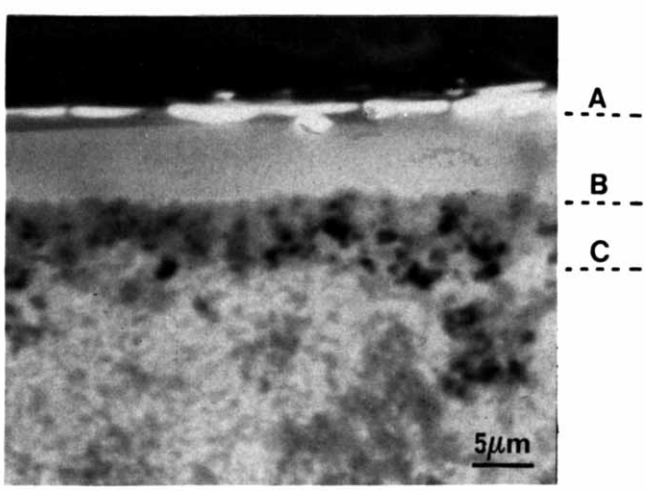

Fig. 4. A duplex scale structure developed after ~20–50 h at 1350°C. The upper part (A) consists of $Y_2Si_2O_7$ crystals in a Si-rich amorphous phase. Layer B close to the matrix/oxide interface is a mixed silicate amorphous region. A cation depletion layer C was identified below the matrix–oxide interface.

oxidation temperature. Some gas pores could be seen in the surfaces, implying that the amorphous phase in the scale was of high viscosity, which inhibited the rapid healing of pores from gas eruption. In cross-section it could be seen that the scales, which were up to ~15 μm in thickness after 50 h at the oxidation temperature, had a duplex structure, as is shown in Fig. 4. The ~10 μm layer closest to the matrix–oxide interface was a mixed silicate amorphous layer containing Si, Y, and Al with minor amounts of the impurity cations Fe, Na and K. The upper layer in contact with air contained $Y_2Si_2O_7$ crystals embedded in a Si-rich amorphous phase.

SEM–EPMA line scans taken through the scale to a distance of 10 μm into the matrix showed that the Y content was highest in the outer part of the duplex scale and decreased continually up to a distance of approximately 5 μm below the oxide scale whereupon it increased to the bulk level again. The Al content was low in the outer part of the scale, high in the amorphous mixed silicate region and decreased significantly for a distance of 5 μm into the bulk material. The Si content increased steadily from the outer part of the scale inwards into the specimen. Thus a zone depleted of cations approximately 5 μm in thickness existed below the matrix–oxide scale interface.

3.3.2 ≥ 1400°C

The oxidation behaviour at temperatures of 1400°C or above was similar for both materials A and B. The oxide scales of specimens heat-treated at 1400°C and 1500°C for 10 h were found to have a rough, cracked surface (see Fig. 5(a)). X-Ray analysis (Table 3) showed that, in addition to an amorphous phase, the main crystalline phase present in the scale was SiO_2 (α- and β-cristabolite). In cross-section these scales were seen to be of up to 50 μm in thickness (Fig. 5(b)). These porous scales were evidently non-protective and the material oxidised to such an extent that after 50 h at 1400°C it was frequently found that the whole specimen had been consumed. When heat-treated at 1500°C for 50 h the material was frequently found to melt.

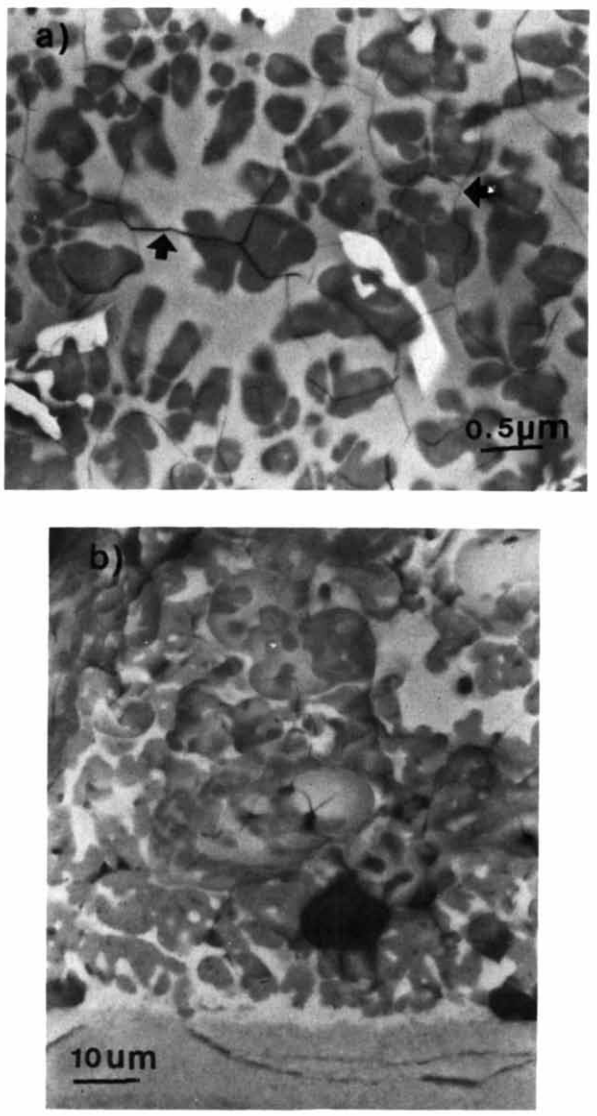

Fig. 5. SEM backscattered images of material oxidised at 1400°C for 10 h: (a) surface view and (b) transverse section. (a) The scale surface was cracked (arrows) and only small amounts of crystalline $Y_2Si_2O_7$ were present. (b) Porosity in the oxide scale and sub-scalar cracking.

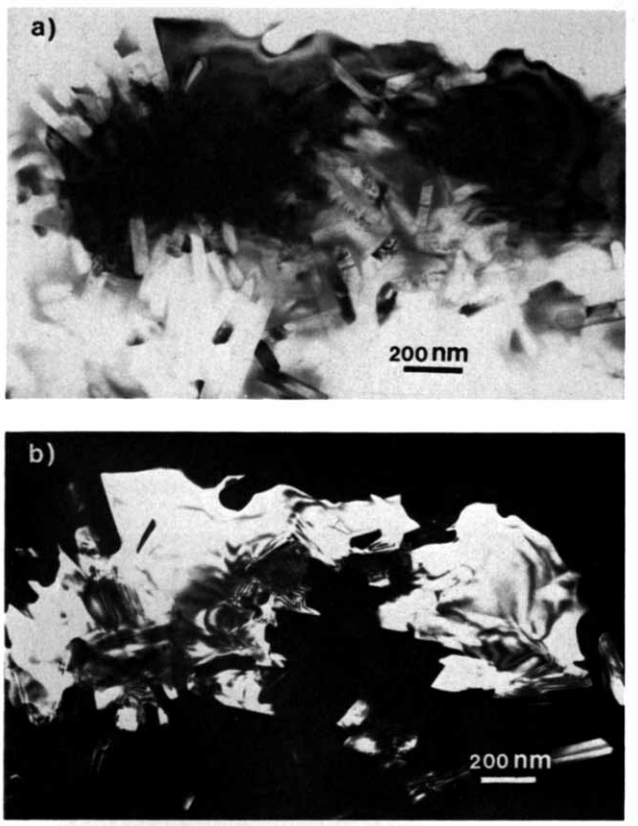

Fig. 6. TEM of a multigrain $Y_2Si_2O_7$ region in material A. (a) Bright field and (b) dark field using a $Y_2Si_2O_7$ diffracted beam.

3.4 Internal microstructural changes

3.4.1 1200°C and 1350°C

TEM revealed that heat-treatment in air at temperatures in this range for 20 and 50 h resulted in considerable crystallisation of the glassy phase which was present in the as-sintered microstructures of materials A and B. The main crystalline phase to develop, as identified by electron and X-ray diffraction, was $Y_2Si_2O_7$. This phase was found to crystallise as both small isolated grains between the Si_2N_2O crystals and large multi-grain $Y_2Si_2O_7$ regions of up to 5 μm in extent (Fig. 6). However, small glass pockets could still be found in the microstructures of materials A and B after both 20 and 50 h at the oxidation temperature. This glass phase was not phase separated and EDX analysis showed that the glassy pockets contained mainly Y, Si and Al. In addition, continuous thin films of glass ($\sim$10–50 Å) surrounded the crystals as is shown in the lattice fringe, and dark-field TEM images of Figs 7 and 8. At 1200°C more extensive crystallisation of the intergranular glass was observed after 50 h as compared to 20 h. However, at 1350°C, no significant difference could be detected between the microstructures of specimens oxidised for 20 or 50 h. Evidence for internal oxidation was observed in material A which had the most extensive as-sintered residual porosity. The pores were filled or partly filled with a Si-rich amorphous phase (Fig. 9). A greater density of Si_2N_2O crystals of sub-micron size was noted in material B than in the as-sintered material. This observation implies that continued nucleation and growth of this phase occurred during heat-treatment of this material.

3.4.2 $\geq$1400°C

Examination of material oxidised at 1400°C and 1500°C for 10 h by TEM revealed that no crystallisation of the remnant intergranular glass phase had taken place. On the contrary, the volume of glass in the microstructure was found to increase at the expense of the Si_2N_2O crystalline phase (Fig. 10). The amorphous material was markedly phase

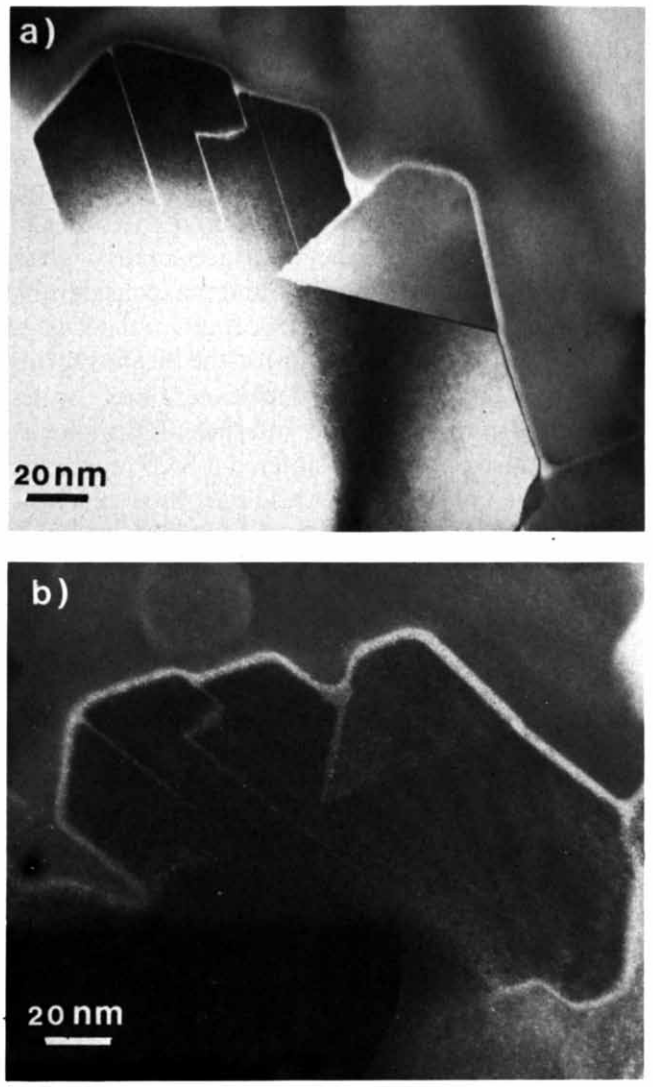

Fig. 7. Thin amorphous films between the Si_2N_2O (S) crystals and $Y_2Si_2O_7$ (Y) grains. TEM micrographs showing (a) bright field and (b) dark field image using diffuse scattered electrons.

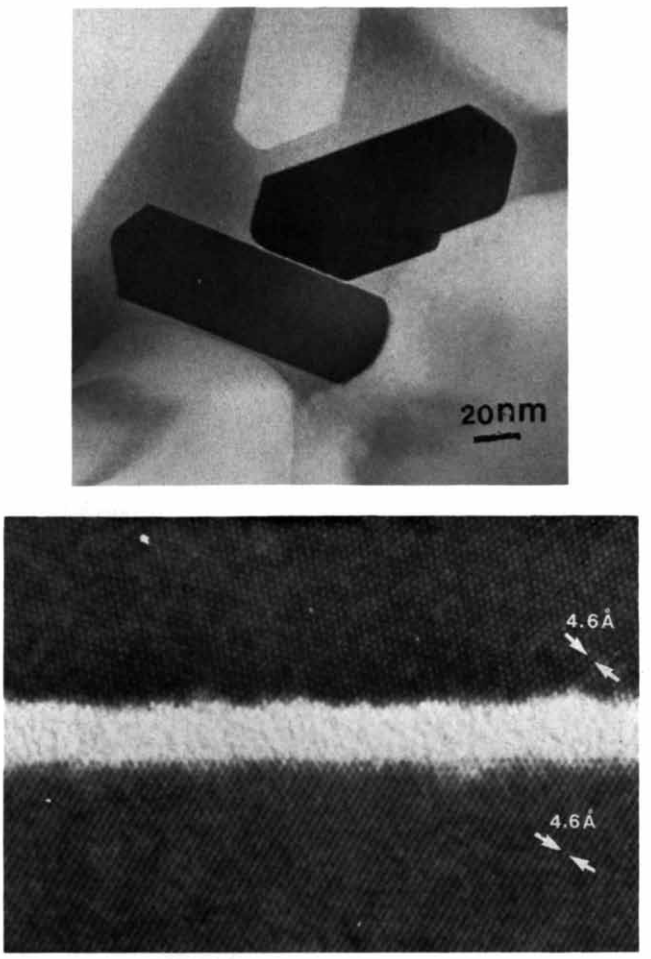

Fig. 8. Lattice fringe TEM image showing the presence of a thin amorphous film (~ 4 nm) between two Si_2N_2O crystals. The lattice images corresponds to the (110) planes in both crystals (spacing 4·68 Å).

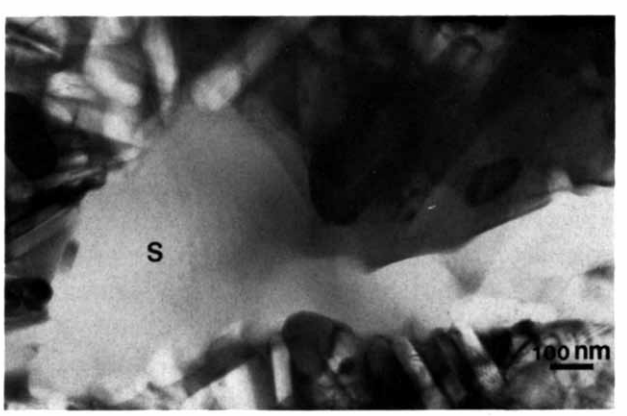

Fig. 9. TEM micrograph of an internal pore in material A filled with a Si-rich amorphous phase (S) after heat treatment at 1200°C for 20 h.

separated, as is shown in Fig. 11, where separate Y-rich and Si-rich glass phases surrounded a small Si_2N_2O crystal. This liquid-phase separation had the morphology of metastable immiscibile liquid phases,[16] indicating that the separation had probably occurred during cooling from the heat-treatment temperature. After 20 h at 1400°C large areas of the specimens were devoid of any crystalline phase.

4 Discussion

At temperatures ≤ 1100°C negligible weight gain of the specimens was recorded following oxidation. This result is surprising with respect to the amount of intergranular glass phase present in the microstructure and the fact that it has been shown that oxidation of the pure Si_2N_2O phase begins at ~ 1100°C.[11] Apart from acting as a high-diffusivity path for oxygen to the internal pores of the material, the amorphous phase can itself be rapidly oxidised at this temperature.

The oxidation behaviour of the materials which had undergone microstructural analysis is most

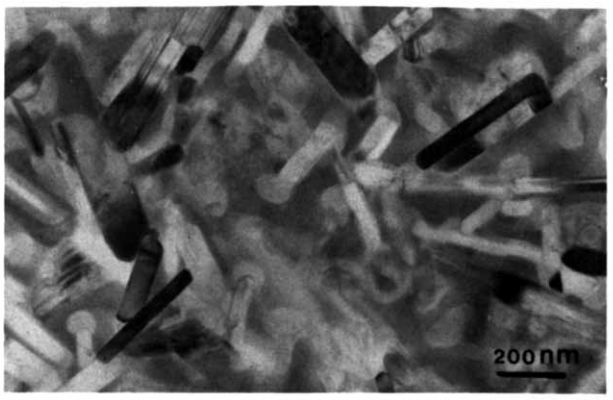

Fig. 10. Increased volume of glass in the microstructure of material A after heat treatment at 1400°C for 10 h.

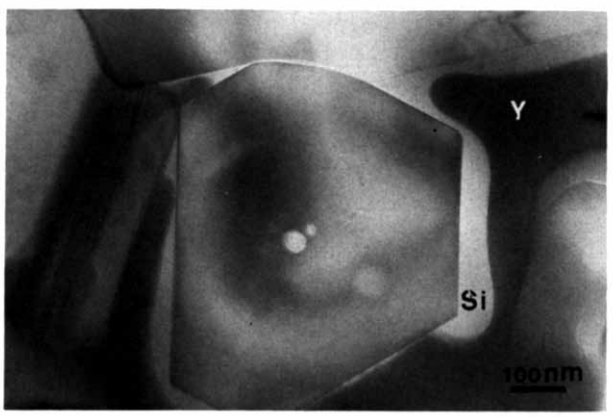

Fig. 11. Phase separation into immiscible glassy Y-rich (Y) and Si-rich (Si) regions in the microstructure of material B heat treated at 1400°C for 10 h.

conveniently discussed in the temperature groupings outlined in Section 3.

4.1 Oxidation and crystallisation at 1200°C and 1350°C

Both materials exhibited excellent oxidation resistance at these temperatures with the formation of thin continuous protective scales which developed a duplex morphology after long exposures. The percentage weight increases recorded after 50 h oxidation are not consistent with the formation of thin ($\sim 15\,\mu$m) oxide films. This indicates that a considerable amount of internal oxidation must have taken place. TEM revealed partial filling of the internal pores with an Si-rich amorphous phase which most probably arose because of internal oxidation. This behaviour is very similar to that which has been observed in RBSN materials where the oxidation kinetics are best described by an asymptotic law due to the slow but nevertheless continued oxidation of both the internal pores and the specimen surface after a high initial internal oxidation reaction.[17] The weight gain for material A was slightly higher than that for material B, reflecting the higher open porosity of the material which had been prepared from amorphous starting powder.

Lewis & Bernard[18] suggested that the excellent oxidation resistance of similar Si_2N_2O materials at temperatures up to 1350°C is due to a rapid suppression of outward diffusion of yttrium by crystallisation of the near-surface matrix glass. However, in this work it was found that considerable diffusion of Y, Al and impurity cations had occurred from the bulk material into the scale during oxidation and a cation depletion zone formed beneath the matrix–oxide interface. This phenomenon is also observed in sintered β-Si_3N_4 materials where it is considered to result from a 'reaction-couple' established between the amorphous oxide scale and the amorphous intergranular phase.[19,20] This reaction-couple operates to decrease the chemical gradient between the two phases. As observed in the present work the outward diffusion of cations (Y and Al) to the external oxide layer results in the formation of mixed silicate scales from which $Y_2Si_2O_7$ crystals nucleate and grow. After ~ 20 h of oxidation a duplex scale forms. Thus, as is shown by the oxidation of internal pores and the build up of N_2 bubbles at the material–oxide interface, cation diffusion occurs outwardly from the sub-scalar material and oxygen diffuses inwards.

A duplex scale has also been observed to develop during the oxidation of β'-sialon materials and this was attributed to being the reason for the improved oxidation resistance of these materials.[21] It has also been suggested that the high concentration of the intermediate network former, Al^{3+}, in the lower glassy portion of the scale, as was also found in this work, counters the viscosity-reducing effects of the Y^{3+} and impurity ions.[18,22] The scale thus maintains a high glass viscosity close to the matrix–oxide interface and this may inhibit inward diffusion of oxygen and so reduce the overall rate of oxidation.

Although the major part of the grain boundary glass phase was transformed to crystalline $Y_2Si_2O_7$ during oxidation at these temperatures, small quantities of glass were still present in the microstructure after 50 h at the heat-treatment temperature. Furthermore, after heat-treatment at 1350°C, no significant decrease in the amount of this thin grain boundary phase could be observed when comparing 20 and 50 h treatments. This observation is in agreement with the theoretical predictions of Raj & Lange[23] that grain boundary amorphous films and small glass pockets may not be able to crystallise due to the elastic constraint imposed by the surrounding crystalline phase. The volume strain

energy associated with crystallisation of the glass phase opposes the transformation, and therefore a glass pocket must be above a certain minimum size if crystallisation is to take place. Clarke[24] proposes that since amorphous films wetting the grain boundaries reduce their interfacial energy, an equilibrium thickness of grain boundary films of dimensions similar to those found in this work (1–2 nm) will eventually be reached and further removal of the glassy films will be very difficult.

At these temperatures no significant difference was observed in the oxidation behaviour of materials A and B. This implies that the difference in their microstructural features, such as grain size distribution and residual porosity, plays only a minor role in influencing the oxidation resistance in this temperature range. However, both materials, in the as-sintered form, contained significant quantities of an amorphous intergranular phase and it is this microstructural feature which strongly influences the oxidation behaviour.

4.2 Oxidation at temperatures $\geq 1400°C$

The rough, porous nature of the oxide scales, the large weight gains and the total consumption of the specimens after longer periods of oxidation are consistent with a catastrophic oxidation process at temperatures $\geq 1400°C$. It was first thought that this behaviour could be due to the decomposition of Si_2N_2O. However, decomposition should only occur at high P_{N_2}/P_{O_2} and it should be accompanied by specimen weight loss. In order to interpret the oxidation behaviour it should be recalled that the volume of glass in the microstructure increased with time at the oxidation temperature and that the material frequently melted when exposed at 1500°C for a long time. It is therefore most probable that at these temperatures, the rapid inward diffusion of oxygen through the amorphous grain boundary phase and the concurrent outward diffusion of cations to the oxide scale resulted in a shift of the bulk composition into a liquid-forming region of the Y–Si–Al–O–N system. The results of recent work[25] indicate that the eutectic melting temperature of this liquid-forming region occurs at ~1375°C (Fig. 12). Therefore melting occurs within the material as oxidation progresses. At 1400°C an oxide scale is formed and although it is non-protective it slows down the inward diffusion of oxygen and extensive melting occurs in the bulk material. The liquid phase which forms probably has a very high viscosity and on cooling from the oxidation temperature it separates, below the liquidus, into immiscible Y-rich and Si-rich liquid phases. At 1500°C the specimens

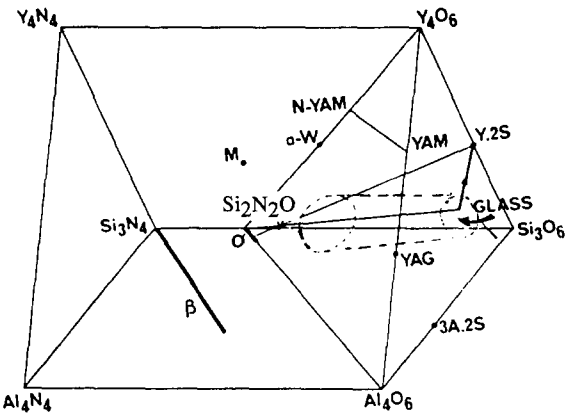

Fig. 12. The Jänecke prism representation of the Y–Si–Al–O–N system showing the relationship between Si_2N_2O, the end components, e.g. Si_3N_4 and the eutectic liquid zone (after Lewis *et al.*[8]).

were observed to melt and this behaviour is consistent with the occurrence of a eutectic in the SiO_2–$Y_2Si_2O_7$–Si_2N_2O system at ~1500°C.[27]

5 Conclusions

(1) Because of the formation of thin (~15 μm) protective oxide scales, pressureless sintered Si_2N_2O exhibited excellent resistance to oxidation by air at temperatures up to 1350°C.

(2) The oxide scale developed a duplex morphology during oxidation at temperatures of 1200 and 1350°C.

(3) Additive (Y, Al) and impurity (Fe, K, Na) cations accumulated in an amorphous region of the duplex scale close to the matrix–oxide interface. The outer region of the scale consisted of $Y_2Si_2O_7$ crystals embedded in a Si-rich glassy phase. A sub-scalar zone (~5 μm) in the bulk material was depleted of cations.

(4) Heat-treatment in air at the temperatures of 1200 and 1350°C resulted in substantial crystallisation of the intergranular glassy phase with extensive formation of $Y_2Si_2O_7$. Small glassy pockets and thin (1–5 nm) intergranular glassy films remained in the microstructure.

(5) Catastrophic oxidation was observed at temperatures greater than 1350°C. This behaviour was enhanced by an oxidation-induced shift in the composition of the bulk material to a liquid-forming region in the Y–Si–Al–O–N system where a eutectic melting temperature occurs at ~1375°C.

Acknowledgements

Lars Eklund of the Swedish Institute for Silicate Research is gratefully acknowledged for help with analysis by SEM–EPMA. Financial support by the Swedish Board for Technical Development is also gratefully acknowledged.

References

1. Washburn, M. E., Silicon oxynitride refractories. *Am. Ceram. Soc. Bull.*, **46**(7) (1967) 667–71.
2. Billy, M., Boch, P., Dumazeau, C., Glandus, J. C. & Goursat, P., Preparation and properties of new silicon oxynitride based ceramics. *Ceramics International*, **7**(1) (1981) 13–18.
3. Ohashi, M., Tabata, H. & Kansaki, S., Mechanical properties of hot-pressed silicon oxynitride ceramics. In *Sintering '87*, Tokyo, 4–6 November 1987, Elsevier Applied Science.
4. Huang, Z. K., Greil, P. & Petzow, G., *Ceramics International*, **10** (1984) 14–17.
5. Boch, P. & Glandus, J. C., *J. Mater. Sci.*, **14** (1979) 379–85.
6. Ehlert, T. C., Dean, T. P., Billy, M. & Labbe, J.-C., *J. Am. Ceram. Soc.*, **63** (1980) 235–6.
7. Lothary, P. & Billy, M., *Bull. Soc. Chim. Fr.*, **5** (1975) 1057–61.
8. Lewis, M. H., Reed, C. J. & Butler, N. D., *Mater. Sci. Eng.*, **71** (1985) 87–94.
9. O'Meara, C. & Sjöberg, J., The development of microstructure in pressureless sintered Si_2N_2O bodies. In *Ceramic Transactions*, Vol. 7. American Ceramic Society, 1990, pp. 647–63.
10. Blegen, K., Equilibrium and kinetics in the systems Si–N, Si–O–N and Si–C–O–N. Laboratory of Silicate Science, The University of Trondheim, Norway, 1976.
11. Zabruskova, T. N., Guzman, I. Ya. & Dimitriev, I. A., *Refractories*, **2** (1972) 118–21.
12. Lothary, P., Goursat, P., Tédard, D. & Billy, M., *Rev. Int. Hautes T. empér. et Réfract.*, **9** (1972) 325–32.
13. Lange, F. F., Singal, S. C. & Kuznicki, R. C., Phase relationships and stability studies in the Si_3N_4–SiO_2–Y_2O_3 pseudoternary system. *J. Am. Ceram. Soc.*, **60**(5–6) (1977) 249.
14. Sjoberg, J., Rundgren, K., Osten-Sacken, J. & Pompe, R., Nitridation of silica with ammonia: Some important features. In *Science of Ceramics 14*, ed. D. Taylor. The Institute of Ceramics, Stoke-on-Trent, 1988.
15. Sjöberg, J., Preparation of Si_2N_2O from amorphous SiO_2 and NH_3. Report OOK 88:03, Chalmers University of Technology, Göteborg, Sweden, 1988.
16. James, P. F., Review: Liquid phase sintering in glass forming systems. *J. Mater. Sci.*, **10** (1975) 1802–25.
17. Porz, F. & Thummler, F., *J. Mater. Sci.*, **19** (1984) 1283.
18. Lewis, M. H. & Bernard, P., *J. Mater. Sci.*, **15** (1980) 443.
19. Clarke, D. R. & Lange, F. F., *J. Am Ceram. Soc.*, **63** (1980) 586.
20. Clarke, D. R., In *Progress in Nitrogen Ceramics*, ed. F. L. Riley. Martinus Nijhoff, The Hague, 1983, p. 421.
21. Arrol, W. J., In *Proceedings of the 2nd Army Materials Technology Conference*, ed. J. J. Burke, A. E. Gorum & R. M. Katz. Brookhill, Chestnut Hill, 1974, p. 729.
22. Hampshire, S. & Pomeroy, M., In *Proceedings 2nd Irish Durability and Fracture Conference* (1984).
23. Raj, R. & Lange, F. F., *Acta Met.*, **29** (1981) 1993.
24. Clarke, D., *J. Am. Ceram. Soc.*, **70** (1987) 15–22.
25. O'Meara, C., Dunlop, G. L. & Pompe, R., In *Science of Ceramics* 14, ed D. Taylor. The Institute of Ceramics, Stoke-on-Trent, 1988, p. 461.
26. Trigg, M. B. & Jack, K. H., In *Proc. Int. Symp. on Ceramic Components for Engines*, Japan, 1984, pp. 199–207.
27. Gauckler, L. J., Hohnke, H. & Tien, T. Y., *J. Am. Ceram. Soc.*, **63** (1980) 35.